Short Communcation

Biomass Carbon Modified Zinc Anode for Rechargeable Aqueous Batteries

Zinan Ou[1,2], Qiaoni Liu[1,2], Yuxuan Wang[1,2], Guojiang Wu[2,]*

[1] Hefei No.8 High school, 1688 Xiyou Road, Hefei 230071, Anhui, P.R. China.
[2] Institute of Plasma Physics, Hefei Institutes of Physical Science, Chinese Academy of Sciences, Hefei 230031, People's Republic of China
[*]E-mail: gjwu@ipp.ac.cn

Aqueous zinc ion batteries are considered to be potential alternatives for the new energy storage system. The cycle stability of aqueous zinc ion batteries depends on the reversible stripping/plating of Zn on the anode, which is often exacerbated by its uncontrollable dendrite growth and corrosion. Here, we show an easy and low-cost surface coating strategy, which can significantly promote the cycle performance of Zn anode. A biomass carbon coating was innovatively proposed on Zn anode. The Zn electrode cycling stabilities are extended by about 5 times at 1 mA/cm^2. After 100 cycles, the capacity retention rate of the full battery increased from 44% to 69% at the current density of 0.5 A/g.

1. INTRODUCTION

Aqueous zinc ion batteries (AZIBs) have stimulated much research interest because of their inherent safety, low cost and high theoretical capacity (5855 mAh/cm^3) [1]. As energy storage equipment for large-scale systems, they are excellent substitutes for Li-ion batteries. However, uncontrollable dendrite growth, side reactions and hydrogen evolution worsen the zinc electrode interface, resulting in poor coulomb efficiency, short cycle life, and even short circuited fault in AZIBs, which hinders its further development [2]. Many tactics have been dedicated to resolve the above problems. Such as artificial SEI interface [3], electrolyte optimization [4] and electrode design [5] and so forth. Among them, constructing an elaborate artificial interface on Zn anode is an effective method to inhibit Zn dendrites and alleviate the electrolyte corrosion. At present, all sorts of interface layers, including inorganic compounds (CaCO$_3$ [6], TiO$_2$ [7], ZrO$_2$ [8], Al$_2$O$_3$ [9], ZnF$_2$ [10]), carbon materials (CNTs [11], carbon black [12] and graphene [13]), and polymers (polyamide [14] and MOF [15]). As we all

know, carbon materials is an ideal material for SEI, which has high corrosion resistance and good stability in water electrolyte. The conductive and porous carbon coating not only makes the interface electric field evenly distributed due to its large specific surface, but also guides the Zn preferred deposition in the gap of porous carbon rather than vertically growing dendrites. Some related studies have reported that dendrite free zinc anode can be obtained by using graphene as zinc coating. Epitaxial graphene can induce zinc ions to grow preferentially along the (002) crystal plane and effectively inhibit Zn dendrites [16]. Similarly, the Zn electrode coated with CNTs can also efficacious restrict Zn dendrites. The existence of CNTs homogenizes the electric field on the surface of Zn anode. The battery shows good performance in the process of repeated cycle without obvious polarization [11].

Considering the high cost of graphene and CNTs, a biomass carbon coating was innovatively proposed on Zn anode in this paper. The biomass carbon (BC) was obtained from corn flour (CF) by a simple method. It has the advantages of low price, large specific surface, good conductivity and outstanding chemical stability. In addition, the porous structure of biomass carbon helps to construct a consecutive conductive network with sufficient void space to accommodate electro galvanization. The BC/Zn electrodes in the symmetrical battery show a long cycle life (200 hours). After 100 cycles, the capacity retention rate of the full battery increased from 44% to 69% at the current density of 0.5 A/g.

2. EXPERIMENTAL PART

2.1 Fabrication and characterization of BC/Zn anode

Corn flour was purchased from Xin-Liang food flagship store. All chemical reagents were purchased from Sinopharm Chemical Reagent Co. Ltd. Porous activated carbon (PAC) were prepared from BC. Heat BC in a tubular furnace at the rate of 5 °C/min to 500 °C, carbonize and sinter for 1 hour, and then naturally cool down to room temperature. The samples obtained and KOH are mixed in a mass ratio of 1:3. Then put the ground powder mixture into the tubular furnace for sintering. The tubular furnace heats it to 800 °C at the rate of 5 °C/min, and naturally cools it to room temperature after constant temperature for 1 hour. Take out the sintered solid, drop dilute hydrochloric acid until the pH value is 7, then filter and clean. Finally, dry it in the drying oven at 80 °C for all night to obtain PAC.

PAC and polyvinylidene difluoride (PVDF) were mixed with a mass ratio of 9: 1, and N-methylpyrrolidone (NMP) as dispersant. Then the mixture was coated on a Zinc foil. Finally, put it into the drying oven and dry it at 80 °C for 5 hours to obtain BC/Zn anode.

2.2 Fabrication of MnO_2 cathode

Typically, 0.608 g $KMnO_4$ was added to 70 mL deionized water, then put in 1.27 ml HCl and the mixture was stirred for 30 min. The solution was then shifted to the 100 mL Teflon-lined autoclave and maintained 140 °C for 12 h. The final sample was washed with deionized water several times, dried at 80 °C in air [17].

The cathode electrodes were obtained by MnO_2, PVDF and carbon black at a mass ratio of 7:1:2 in NMP. Then, the mixed slurry was coated on the stainless steel mesh and dried at 80 °C, and the loading weight was about 1.2 mg.

2.3 Characterization and electrochemical measurements

The sample morphology was derived by scanning electron microscopy (SEM, GeminiSEM 500). The phase structure of samples was characterized by X-ray diffraction (XRD, Cu Ka, 1.5418 Å).

Galvanostatic cha-discharging (GCD) was measured on Neware testing system (0.8-1.8 V). Electrochemical impedance spectroscopy (EIS) was measured by adopting CHI660e (0.01 Hz- 100 kHz).

2.4 Fabrication of the full batteries

A conventional coin-type AZIBs was assembled using CR2032 cases, with the MnO_2 as cathode, the zinc foil (or BC/Zn) as anode, and the 2 M $ZnSO_4$ and 0.1 M $MnSO_4$ aqueous solution as electrolyte.

3. RESULTS AND DISCUSSION

In this work, MnO_2 was prepared by a hydrothermal method. The XRD spectrum of the synthesized MnO_2 is shown in Fig. 1. All diffraction peaks correspond to α-MnO_2 (JCPDS: 44-0141), and no other characteristic peaks of impurities are observed. This indicates the high purity of MnO_2 sample.
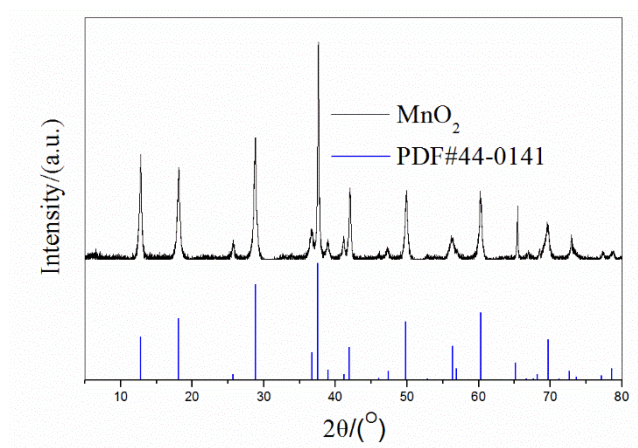
Figure 1. XRD pattern of the synthesized MnO_2

The BC/Zn anode was fabricated by scraper coating the porous activated carbon derived from corn flour on the Zn foil. To evaluate the stability of Zn and BC/Zn electrode during cha-discharging

cycle, the symmetrical coin battery consisting of two identical Zn (or BC/Zn) and aqueous electrolyte of 2 M $ZnSO_4$ was assembled. It can be seen from Fig. 2 that the polarization voltage of Zn||Zn symmetrical battery has been maintained within 0.06 V for 40 hours under the current density of 1 mA/cm^2. After 40 h, the polarization voltage increases gradually with the increase of cycle time. However, the BC/Zn||BC/Zn composite symmetrical battery maintained the polarization voltage within 0.06 V for more than 200 hours at the same current density. The difference between the two symmetrical composite zinc ion batteries is highly interrelated with the effect of collector on the micro morphology of zinc. The reason will be analyzed in detail in the following study. Table 1 lists the comparison of the lifespan in symmetric cells for this work with coating related work. The performance of our materials is better than most of the reported SEI materials, and biomass carbon is rich in resources and low cost, which is a SEI material with great potential for Zn anodes.
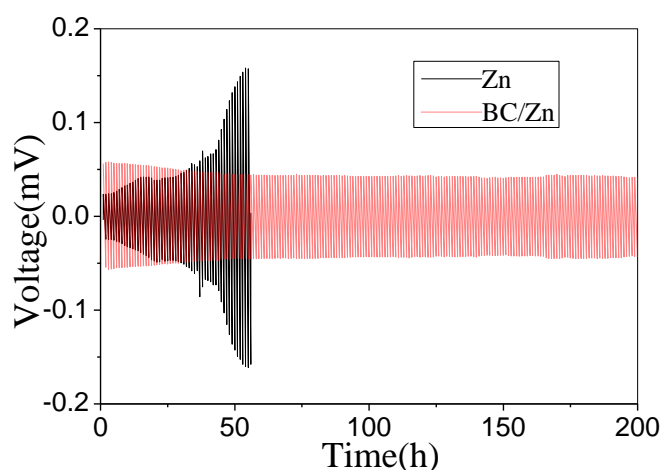

Figure 2. The galvanostatic cyclic curves of Zn symmetrical batteries and BC/Zn symmetrical batteries.

Table 1. Performance comparison for this work with coating related work Zn-based symmetrical cell at the current density of 1.0 mA h cm^{-2} and the capacity of 1.0 mA h cm^{-2} in reported works

| Anode materials	Lifespan (h) Untreated Zn	Lifespan (h) Treated Zn	Ref.
rGO/Zn	108	300	[19]
Al_2O_3/Zn	242	500	[9]
TiO_2/Zn	35-95	150	[20]
Sc_2O_3/Zn	94	200	[21]
MXene/Zn	60	150	[22]
BC/Zn	**40**	**200**	**This work**

The cycle stability of aqueous $Zn-MnO_2$ full batteries based on two kinds of zinc anodes was also examined. As can be shown from Fig. 3, the initial discharge capacity of $BC/Zn\|MnO_2$ battery and $Zn\|MnO_2$ battery are 269.5 mAh/g and 264.5 mAh/g at 0.5 A/g, respectively. After 100 cycles, the capacity of $BC/Zn\|MnO_2$ battery is 186 mAh/g, while that of $Zn\|MnO_2$ battery is only 116.7 mAh/g. The main reason is the anode covered with porous carbon provides a stable deposition site for the zinc, and the interface electric field evenly distributed due to its abundant specific surface [11]. Therefore, the deposition and stripping of zinc are higher stability during the process of charge and discharge, which improves the stability of zinc ion battery.

In order to further study the reasons for the difference of electrochemical stability between the two batteries, a series of experiments were deeply studied, including photography, XRD, SEM and EIS measurements. Before and after 100 cha-discharge cycles, the photographs of anodes and separators are shown in Fig. 4. The surface of initial zinc foil is flat and smooth (Fig. 4(a)). After 100 cycles, obvious zinc dendrites and corrosions appear on the surface of zinc foil (Fig. 4(b)), and dendrites adhere and penetrate through the separator (Fig. 4(c)).
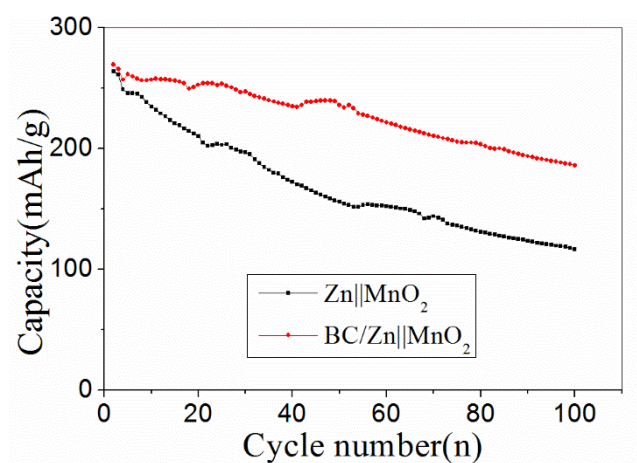
Figure 3. Long-term cycling characteristics of $Zn\|MnO_2$ cells and $BC/Zn\|MnO_2$ cells at 0.5 A/g

Without the modification of porous carbon layer, the dendrite nucleation on the surface of zinc foil will further attract zinc to deposit on the dendrites, resulting in the accumulation and growth of dendrites. In contrast, before and after 100 cycles, there is no obvious change on the BC/Zn surface (Fig. 4(d) (e)).
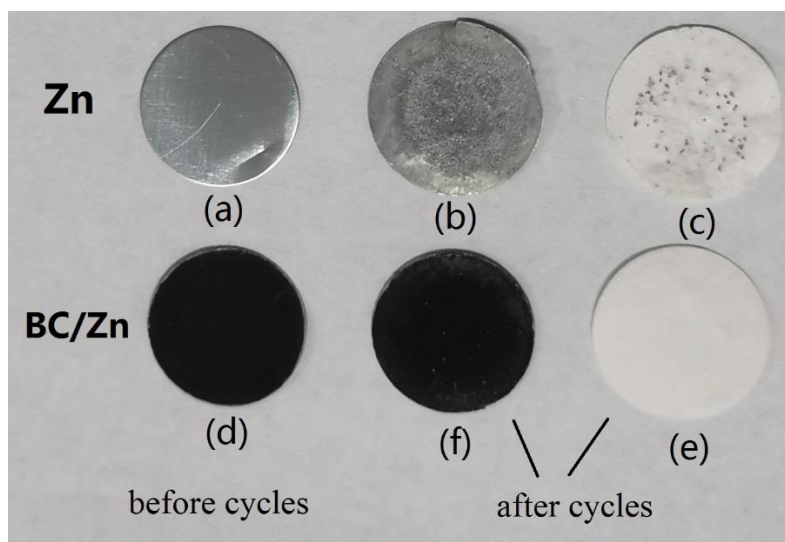
Figure 4. the photographs of anodes and separators (a) Zn anode before cycling ,(b) Zn anode after 100 cycles, and (c) separator after 100 cycles in Zn||MnO$_2$ batteries; (d) BC/Zn anode before cycling ,(e) BC/Zn anode after 100 cycles, and (f) separator after 100 cycles in BC/Zn||MnO$_2$ batteries

After 100 cycles, dendrites are not seen on the surface of the BC/Zn (Fig. 4(e)) and separator (Fig. 4(f)), indicating that the biomass carbon coating inhibits dendrites, which is due to its large surface area adsorption and guiding zinc to preferentially fill the gap between carbon particles, rather than the vertical growth of dendrites. The morphology change on the surface of Zn and BC/Zn electrodes was reconfirmed with the SEM result. As can be seen from Fig. 5(a), the original Zn foil displays a flat and smooth surface. After 100 cycles, many thick and big massive products appear on the surface of Zn electrode (Fig. 5(b)), which is a good response to zinc dendrites. In contrast, the BC/Zn electrode remains non-dendritic after cycles (Fig. 5(d)), on account of relatively homogeneous Zn stripping/plating process. After coating a biomass carbon layer, the surface of BC/Zn is much rougher with a lot of voids (Fig. 5(c)), leaving abundant space for zinc deposition and release during the cycle. Of note, comparing with before cycle, there are many ultrathin nanosheets uniformly grown on the surface of PAC layer, which are by-products during the discharge. To clarify the by-products, The XRD patterns of Zn and BC/Zn anodes after cycles are studied (Fig. 6). And some new peaks are observed after 100 cycles for the Zn and BC/Zn anodes. Based on the XRD analysis, these new peaks can be identified as Zn$_4$SO$_4$(OH)$_6$•5H$_2$O (JCPDS 39-0688) [18].

EIS testing of Zn cells was conducted before and after 100 cycles. As shown in Fig. 7, after 100 cycles, the electron-transfer resistance (R$_{ct}$) of both batteries increases, which is due to the emergence of by-products ((Zn$_4$SO$_4$(OH)$_6$•5H$_2$O) on the electrode surface after cycling, which increases R$_{ct}$. At the same time, comparing R$_{ct}$ of two types of full cell after cycling, the R$_{ct}$ of Zn||MnO$_2$ cells rises from 9.3 Ω before cycling to 51.4 Ω after 100 cycles. Such a large growth may be due to the formation of a great quantity dendrites on Zn anode that interferes with the charge transfer at the interface. Encouragingly, the R$_{ct}$ of BC/Zn||MnO$_2$ cells with BC/Zn anode only increases from 4.8 to 10.8 Ω. According to the SEM analysis, the result can be attributed that the BC coating inhibits dendrites, due to its large surface
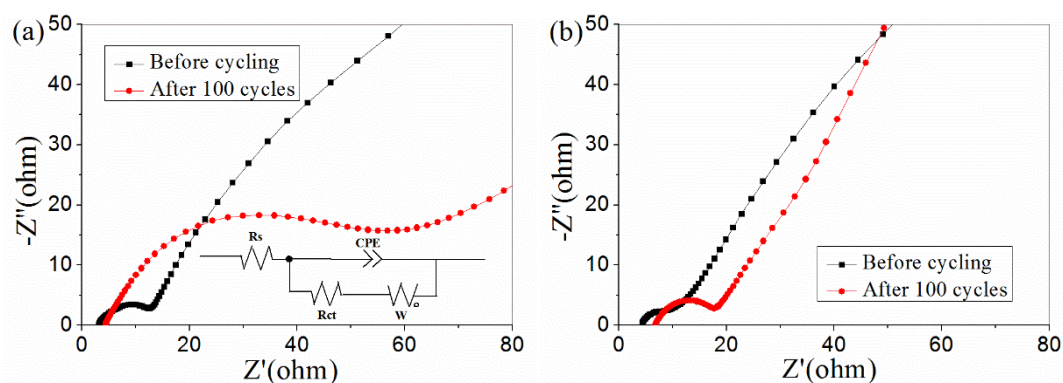
area adsorption and guiding zinc to preferentially fill the gap between carbon particles, rather than the vertical growth of dendrites.
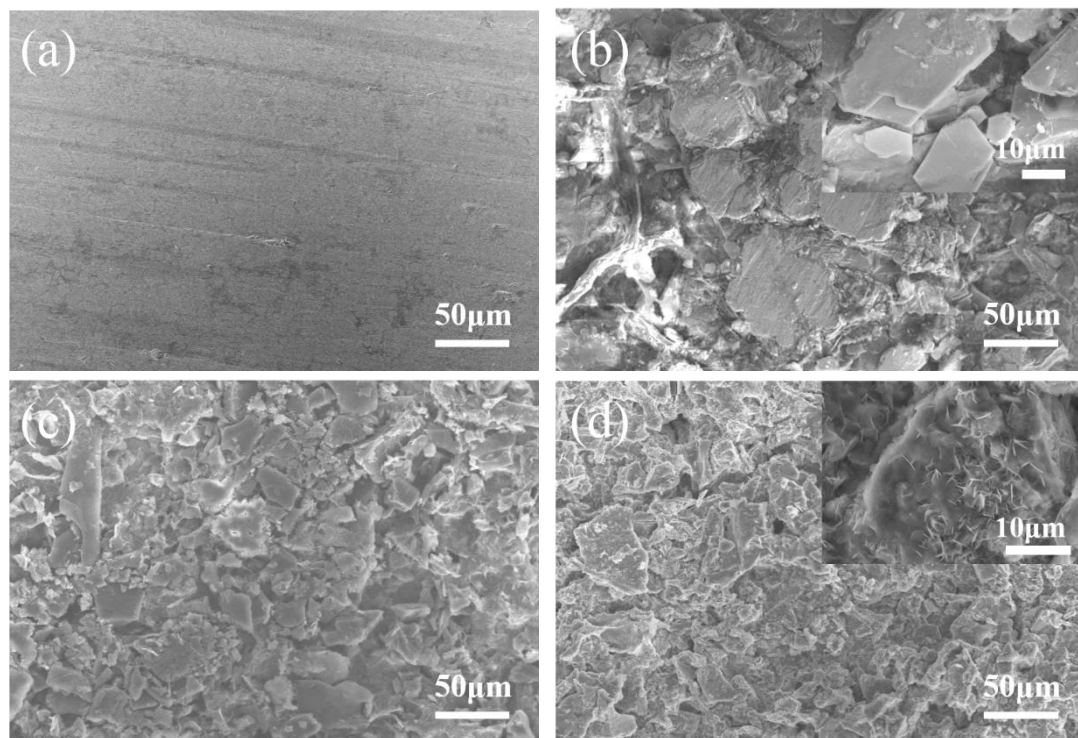
Figure 5. SEM image of Zn and BC/Zn anodes (a) Zn anode before cycling (b) Zn anode after 100 cycles (c) BC/Zn anode before cycling (d) BC/Zn anode after 100 cycles
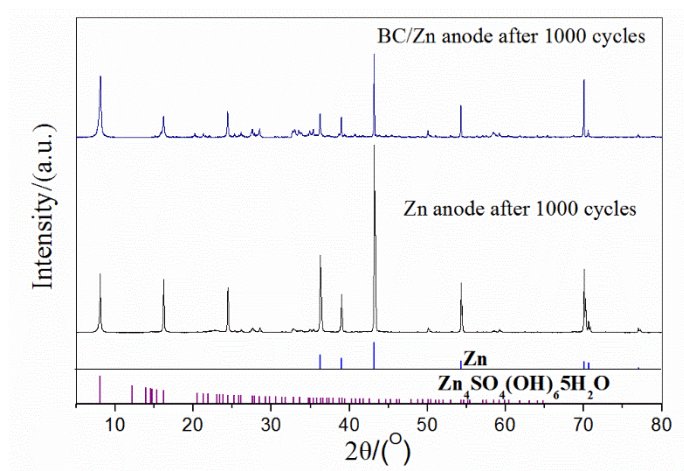
Figure 6. XRD patterns of Zn and BC/Zn anodes after 100 cha-discharge cycles

Figure 7. The EIS results before cycling and after 100 cycles. (a) Zn‖MnO_2 batteries, (b) BC/Zn‖MnO_2 batteries

According to the above analysis, the fast capacity loss of Zn‖MnO_2 battery with untreated anode originates from the Zn dendrites and corrosions on the anode surface. As for BC/Zn‖MnO_2 battery with biomass carbon coating, the anode surface hardly changed, indicating that the biomass carbon coating can effectively restrict dendrites. Therefore, the stability of the battery is significantly improved.

4. CONCLUSIONS

In summary, without the modification of biomass carbon layer, the dendrite nucleation on the surface of zinc foil will further attract zinc to deposit on the dendrites, resulting in the accumulation and growth of dendrites. Encouragingly, the dendrite can be inhibited effectively on the surface of Zn anode with a biomass carbon coating. The porous structure of biomass carbon not only helps to construct a consecutive conductive network with sufficient void space to promote the interface electric field evenly distributed, but also its large surface area adsorption and guiding zinc to preferentially fill the gap between carbon particles, rather than the vertical growth of dendrites. A simple processing of Zn anode with the biomass carbon layer evidently improved the uniformity of Zn^{2+} deposition/dissolution process, and promoted cycle life of AZIBs. The Zn electrode cycling stabilities are extended by about 5 times at 1 mA/cm^2. In the electrochemical performance test of the coin cells, BC/Zn‖MnO_2 composite zinc ion battery shows higher capacity and stability than Zn‖MnO_2 battery. The strategy should be beneficial to the practical manufacture of high stability AZIBs.

References

1. L.E. Blanc, D. Kundu, L.F. Nazar, *Joule*, 4 (2020) 771-799.
2. W.C. Du, E.H.X. Ang, Y. Yang, Y.F. Zhang, M.H. Ye, C.C. Li, *Energy & Environmental Science*, 13

(2020) 3330-3360.
3. S.H. Park, S.Y. Byeon, J.H. Park, C. Kim, *Acs Energy Letters*, 6 (2021) 3078-3085.
4. G. Chang, S.J. Liu, Y.N. Fu, X. Hao, W. Jin, X.B. Ji, J.G. Hu, *Advanced Materials Interfaces*, 6 (2019) 1901358.
5. W.B. Guo, Z.F. Cong, Z.H. Guo, C.Y. Chang, X.Q. Liang, Y.D. Liu, W.G. Hu, X. Pu, *Energy Storage Materials*, 30 (2020) 104-112.
6. L.T. Kang, M.W. Cui, F.Y. Jiang, Y.F. Gao, H.J. Luo, J.J. Liu, W. Liang, C.Y. Zhi, *Advanced Energy Materials*, 8 (2018) 1801090.
7. X.Y. Zhou, P.H. Cao, A.R. Wei, A.T. Zou, H. Ye, W.P. Liu, J.J. Tang, J. Yang, *Acs Applied Materials & Interfaces*, 13 (2021) 8181-8190.
8. P.C. Liang, J. Yi, X.Y. Liu, K. Wu, Z. Wang, J. Cui, Y.Y. Liu, Y.G. Wang, Y.Y. Xia, J.J. Zhang, *Advanced Functional Materials*, 30 (2020) 1908528.
9. H.B. He, H. Tong, X.Y. Song, X.P. Song, J. Liu, *Journal of Materials Chemistry A*, 8 (2020) 7836-7846.
10. L. Ma, Q. Li, Y. Ying, F. Ma, S. Chen, Y. Li, H. Huang, C. Zhi, *Advanced Materials*, 33 (2021) 2007406.
11. M. Li, Q. He, Z.L. Li, Q. Li, Y.X. Zhang, J.S. Meng, X. Liu, S.D. Li, B.K. Wu, L.N. Chen, Z. Liu, W. Luo, C.H. Han, L.Q. Mai, *Advanced Energy Materials*, 9 (2019) 1901469.
12. A.R. Wang, W.J. Zhou, A.X. Huang, M.F. Chen, J.Z. Chen, Q.H. Tian, J.L. Xu, *Journal of Colloid and Interface Science*, 577 (2020) 256-264.
13. J.H. Zhou, M. Xie, F. Wu, Y. Mei, Y.T. Hao, R.L. Huang, G.L. Wei, A.N. Liu, L. Li, R.J. Chen, *Advanced Materials*, 33 (2021) 2101649.
14. Z.M. Zhao, J.W. Zhao, Z.L. Hu, J.D. Li, J.J. Li, Y.J. Zhang, C. Wang, G.L. Cui, *Energy & Environmental Science*, 12 (2019) 1938-1949.
15. X.C. Pu, B.Z. Jiang, X.L. Wang, W.B. Liu, L.B. Dong, F.Y. Kang, C.J. Xu, *Nano-Micro Letters*, 12 (2020) 152.
16. J.X. Zheng, Q. Zhao, T. Tang, J.F. Yin, C.D. Quilty, G.D. Renderos, X.T. Liu, Y. Deng, L. Wang, D.C. Bock, C. Jaye, D.H. Zhang, E.S. Takeuchi, K.J. Takeuchi, A.C. Marschilok, L.A. Archer, *Science*, 366 (2019) 645-648.
17. W. Xiao, H. Xia, J.Y.H. Fuh, L. Lu, *Journal of Power Sources*, 193 (2009) 935-938.
18. X. Guo, J. Zhou, C.L. Bai, X.K. Li, G.Z. Fang, S.Q. Liang, *Materials Today Energy*, 16 (2020) 100396.
19. A.L. Xia, X.M. Pu, Y.Y. Tao, H.M. Liu, Y.G. Wang, *Applied Surface Science*, 481 (2019) 852-859.
20. K.N. Zhao, C.X. Wang, Y.H. Yu, M.Y. Yan, Q.L. Wei, P. He, Y.F. Dong, Z.Y. Zhang, X.D. Wang, L.Q. Mai, *Advanced Materials Interfaces*, 5 (2018) 1800848.
21. M. Zhou, S. Guo, G.Z. Fang, H.M. Sun, X.X. Cao, J. Zhou, A.Q. Pan, S.Q. Liang, *Journal of Energy Chemistry*, 55 (2021) 549-556.
22. N.N. Zhang, S. Huang, Z.S. Yuan, J.C. Zhu, Z.F. Zhao, Z.Q. Niu, *Angewandte Chemie-International Edition*, 60 (2021) 2861-2865.